PHYSICAL REVIEW B **79**, 134109 (2009)

Room-temperature ferromagnetism and ferroelectricity in Fe-doped $BaTiO_3$

B. Xu,[1] K. B. Yin,[1] J. Lin,[1] Y. D. Xia,[1] X. G. Wan,[2] J. Yin,[2,*] X. J. Bai,[2] J. Du,[2] and Z. G. Liu[1]
[1]*Department of Materials Science and Engineering and National Laboratory of Solid State Microstructures, Nanjing University, Nanjing 210093, People's Republic of China*
[2]*Department of Physics and National Laboratory of Solid State Microstructures, Nanjing University, Nanjing 210093, People's Republic of China*

(Received 31 January 2008; revised manuscript received 8 February 2009; published 16 April 2009)

We report the ferroelectricity and ferromagnetism coexistence in the Fe-doped $BaTiO_3$. Our first-principles calculation based on the density-functional theory predicted a magnetic moment of $3.05\mu_B$ per Fe atom when Fe substitutes Ti in $BaTiO_3$, and a ferromagnetic coupling among the magnetic moments of the Fe dopants by using LSDA+U method. The theoretical prediction was confirmed experimentally. The Fe-doped $BaTiO_3$ ceramics prepared by the solid-state-reaction method show simultaneously the ferromagnetic order with the magnetic transition temperature over 680 K and the ferroelectric order with the dielectric transition temperature about 365 K, respectively. The measured magnetic moment about $0.75\mu_B$/Fe atom was smaller than that of the theoretical prediction, and the remnant polarization 2 Pr is about 22.2 $\mu C/cm^2$.

DOI: 10.1103/PhysRevB.79.134109 PACS number(s): 75.80.+q, 75.50.Gg, 77.80.−e, 71.15.Mb

The preparation of a material with simultaneous ferroelectricity and ferromagnetism would be a milestone for modern electronics and functionalized materials. The magnetoelectric multiferroic (MF) materials provide the opportunity to encode information in electric polarization and magnetization to obtain four logic states.[1,2] Until now, many MF materials, such as boracites,[3] $BiFeO_3$,[4] $CdCr_2S_4$,[5] $LuFe_2O_4$,[6] $RMnO_3$, and RMn_2O_5 (R=rare earth, Y, and Bi),[7–11] have been reported. At room temperature, however, the candidate of MF materials is very limited because most of the currently known materials exhibit a low magnetic transition temperature in contrast to a high ferroelectric transition temperature.[12–14] To find other new MF materials with the magnetic and ferroelectric transition temperatures above the room temperature is of both fundamental and technological importance.

We design the room-temperature MF materials by doping the ferroelectric oxide with transition-metal ions as it has been done in the diluted magnetic semiconductors (DMS). It is recently known that DMS, which are the wide-band-gap semiconductors doped with transition-metal ions, such as $Zn_{1-x}Co_xO$, $Sn_{1-x}Co_xO_{2-\delta}$, $Ti_{1-x}Co_xO_{2-\delta}$, and (Ga,Mn)As,[15–18] are very "hot" magnetic materials with the room-temperature ferromagnetism. Most of the perovskite ferroelectrics are usually wide-band-gap semiconductors, such as $BaTiO_3$, $PbTiO_3$, $SrBi_2Ta_2O_9$, and $Pb(Zr,Ti)O_3$. Therefore, we may develop room-temperature MF materials by doping the ferroelectric materials with transition-metal ions.

$BaTiO_3$ is an important and typical ferroelectric material with the band gap about 3.8 eV and the ferroelectric-paraelectric transition temperature above 400 K, and it has been an active subject of research for many years due to its ferroelectricity. Chao *et al.*[19] presented the electronic property of Fe-doped $BaTiO_3$ by the LDA method but they did not consider the magnetic property. In this work, we report our computational and experimental studies on the Fe-doped $BaTiO_3$ ceramics, and it shows both ferroelectricity and ferromagnetism at room temperature.

The first-principles calculation based on the density-functional theory were carried out to investigate the electronic and magnetic properties in the Fe-doped $BaTiO_3$. The calculations were performed by using projector augmented wave (PAW) potentials[20] as implemented in the Vienna *ab initio* simulation package.[21–23] We approximated the exchange-correlation functional with the fully localized limit of the LSDA+U method.[24] Here we use the typical values of U=4.5 and J=0.5 eV on Fe atom. The system was modeled with a periodic supercell of $2\times2\times4$ with 16 formal units (f.u.) of $BaTiO_3$, to form $BaTi_{09375}Fe_{0.0625}O_3$. The Brillouin-zone integrations are performed on a well converged grid of $8\times8\times8$ k points. An energy cutoff of 450 eV was used for the plane-wave expansion of the electronic wave function. Good convergence was obtained with these parameters, with the total energy converged to 1×10^{-5} eV/atom. Density of states (DOS) was calculated by using the linear tetrahedron method with Blöchl corrections. The structure of Fe-doped $BaTiO_3$ was fully relaxed in our LSDA+U calculation by using the conjugate gradient method until the Hellman-Feynman force was smaller than 0.01 eV/Å.

We present the LSDA+U results about the $BaTi_{1-x}Fe_xO_3$. We began by calculating the total energies of $BaTi_{1-x}Fe_xO_3$ with x=0.125 with the LSDA+U approximation by using typical values of U=4.5 and J=0.5 eV on Fe atom. By keeping the volume of $BaTi_{0.875}Fe_{0.125}O_3$ fixed at the experimental volume of $BaTiO_3$, we first relaxed all internal coordinates for the nearest, the second-nearest, and the farthest arrangements of the Fe atom, and for both the ferromagnetic and antiferromagnetic orderings. To investigate the interaction between the magnetic moments, we carried out the calculations with two Ti atoms substituted by Fe atoms in the supercell, corresponding to a doping concentration of 12.5%. It was found that the ferromagnetic ordering is the ground state and its energy is 62.9 meV lower than that of the antiferromagnetic ordering in the case of the farthest configuration, 119.5 meV lower than that of the antiferromagnetic ordering in the case of the second-nearest configuration, and 126.4 meV lower than that of the antiferromagnetic ordering in the case of the nearest configuration, respectively. So the

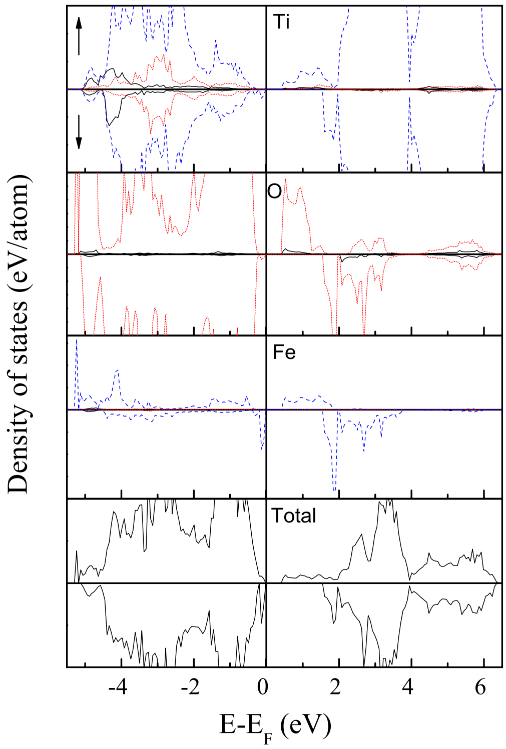

FIG. 1. (Color online) Calculated total (bottom panel) and local density of states for the Fe dopant and the neighboring O and Ti atoms. The Fermi surface is located at $E_f=0$. The blue dotted lines show the *d* states, and the red dashed lines show the *p* states.

ferromagnetic state should be the ground state for all configurations.

Next we presented our calculated DOS of the $BaTi_{0.9375}Fe_{0.0625}O_3$ with the LSDA+U method. Figure 1 shows the total DOS and the projected local densities of states (PDOS) for the dopant Fe and the neighboring Ti and O atoms with the LSDA+U method. The majority (↑) spin states are plotted along the positive *y* direction, and the minority (↓) states are plotted along the negative *y* direction. The energies are plotted relative to the Fermi energy ($E_f=0$). Based on the LSDA+U method, we get a more reasonable result from the Fe-doped $BaTiO_3$ system which is a ferromagnetic semiconductor with the band gap of about 0.41 eV. The blue dotted lines show the *d* states, and the red dashed lines show the *p* states. The strong coupling between the Fe 3*d* orbitals and the O 2*p* orbitals can be observed at the top of the valence band and the bottom of the conduction band. The Ti 3*d* orbitals hybridize with the O 2*p* orbitals near the Fermi surface, as well. The magnetic moment is mainly contributed by the Fe 3*d* orbitals ($3.05\mu_B$) while each of the nearest O and Ti atoms also contributes a little to the magnetic moment ($0.17\mu_B$ and $0.1\mu_B$, respectively), indicating that the hybridization between the Fe 3*d* orbitals and the O 2*p* orbitals is the origin of magnetism in the $BaTi_{0.9375}Fe_{0.0625}O_3$.

To verify our theoretical prediction, $BaTi_{0.95}Fe_{0.05}O_{3-\delta}$ (BTFO) ceramics were prepared by using the solid-state-reaction method with the starting materials of high purity, including $Ba(NO_3)_2$, TiO_2, and Fe_2O_3. The ground and well mixed powder in chemical stoichiometry was preheated at 1000 K for 8 h. The reground powder was sintered at 1200 K for 12 h. The powder sample was then ground, pressed into pellet, heated at 1300 K for 24 h, and cooled to the room temperature with a cooling rate of 5 K/min. Powder x-ray diffraction (XRD) with Cu Kα radiation was employed to characterize the crystal structure of the sample. The microstructure of the BTFO ceramics was studied by using a transmission electron microscope (TEM) (Tecinai F20) with an operating voltage of 200 kV. Detailed high-resolution TEM (HRTEM), the selected area electron-diffraction (SAED), and energy dispersive x-ray (EDX) studies were conducted to investigate the microstructure, respectively. The magnetic properties of the sample were characterized by using a vibrating-sample magnetometer system. The magnetization measurements were taken both as a function of temperature at a fixed field and as a function of the applied magnetic field at the room temperature. The ceramic samples were cut and polished for the measurement of the ferroelectric and dielectric properties. Silver paste was used on both surfaces of the specimen as electrodes. The ferroelectric hysteresis loop was measured by using a RT6000A standardized ferroelectric tester (Radiant Technologies). The dielectric permittivity as a function of temperature was measured with an Agilent 4294A impedance analyzer to determine their ferroelectric-paraelectric transition temperatures.

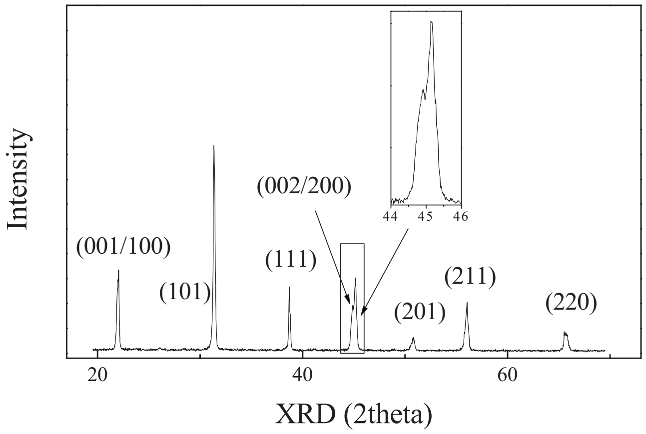

FIG. 2. X-ray diffraction pattern of the $BaTi_{0.95}Fe_{0.05}O_{3-\delta}$ ceramics; the magnification of diffraction peaks in the interval between 44° and 46° in 2θ by the inset.

XRD pattern of BTFO ceramics is shown in Fig. 2. All the diffraction peaks can be indexed, and the phase of tetragonal BTFO is identified by the magnification of diffraction peaks in the interval between 44° and 46° in 2θ as exhibited in inset of Fig. 2. The diffraction peaks (002) and (200) split apparently. The lattice parameters of the BTFO ceramics are determined to be $a=b=4.0138(5)$ Å and $c=4.0331(3)$ Å, respectively. The values of *a* and *b* for the BTFO ceramics exceed those of the pure $BaTiO_3$ ($a=b=3.992$ Å) while the value of *c* for BTFO ceramics is smaller that that of $BaTiO_3$ ($c=4.036$ Å). The c/a ratio (1.0048) of the BTFO ceramics is a little smaller than that of the pure $BaTiO_3$ (1.0107).

The detailed TEM, SAED, and EDX studies were applied to investigate the microstructure of BTFO ceramics and different phases that might have formed in the nanosize range,

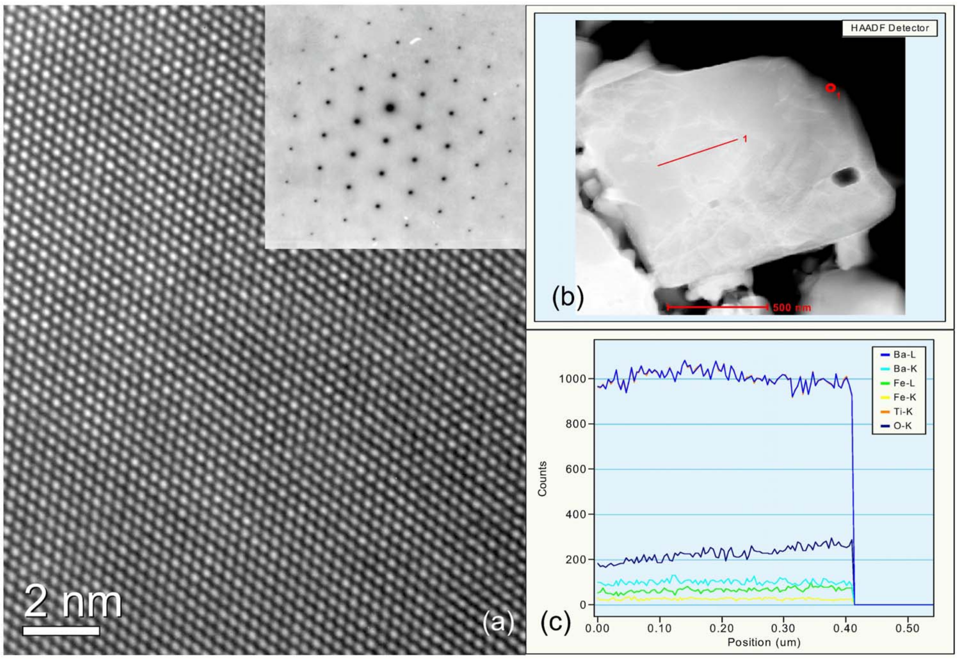

FIG. 3. (Color online) (a) High-resolution transmission electron microscopy of the $BaTi_{0.95}Fe_{0.05}O_{3-\delta}$ ceramics, and selected area electron diffraction in the inset; (b) transmission electron microscopy the $BaTi_{0.95}Fe_{0.05}O_{3-\delta}$ ceramics; (c) energy dispersive x-ray data of each atom along the line in (b).

and to determine the fate of Fe atom which could not be detected by x-ray analysis. The SAED patterns as an inset of Fig. 3(a) as well as the high-resolution micrograph, confirm the high crystalline quality of the BTFO ceramics. The absence of any superstructure reflection in the SAED pattern or defects in HRTEM image indicates the absence of iron oxides or clusters in the sample. Figure 3(b) is the low magnification TEM image of the BTFO ceramic sample. The EDX were both performed at several random points and along a straight line. The EDX data taken at a number of random points throughout the specimens reveal that the concentration of Fe ranges from 4.3–5.4 at. %. As shown in Fig. 3(c), the EDX data shows that Fe is uniformly distributed in a scale of 410 nm with an average concentration of 4.5 at. % along the line in Fig. 3(b). Because of the large difference in the ionic radii between Ba and Fe, Ba prefers to occupy the center of dodecahedron in the perovskite, Fe should occupy the Ti site in $BaTiO_3$ with a coordination number 6.

Ferroelectric property was investigated on the ceramic sample with a thickness of 0.5 mm. Figure 4 exhibits the ferroelectric hysteresis loop measured at a frequency of 2 KHz for the capacitors with the diameter of 0.2 cm at the room temperature, indicating the ferroelectric behavior of the BTFO ceramics. Although the slightly distorted hysteresis loop as observed includes an effect of leakage current, the saturation polarization (P_s) of the ceramic sample at an applied electric field of 125 kV/cm reaches 22 $\mu C/cm^2$, with the remnant polarization (P_r) of 11.1 $\mu C/cm^2$ and the coercive field (E_c) of 37 kV/cm. The discontinuity of the ferroelectric hysteresis loop in Fig. 4 should be ascribed to the special set of the testing voltage pulse in the instrument.

The temperature dependence of the dielectric constant and the loss for the BTFO ceramic sample at different frequencies, ranging from 100 Hz to 1 MHz, are shown in Figs. 5(a) and 5(b), respectively. The peaks were found at 365 K in the curve of both the dielectric constant versus temperature and the dielectric loss curves at all frequencies. It means that the ferroelectric-paraelectric transition (T_{FE}) occurs at 365 K. The ferroelectric transition temperature of the BTFO ceramics is lower than that of the $BaTiO_3$ ceramics, consistent with the result of the Fe-doped $BaTiO_3$ nanoparticles reported by Jana *et al.*[25] The dielectric constant maximum of the BTFO ceramics is much smaller than that of the pure $BaTiO_3$.[26] The response of the dipoles in the sample decreases as the frequency increases because some of the dipoles in the sample are incapable of polarization, following the fast electric-field variations at the high frequency.

As given in Fig. 6, the magnetization-temperature (M-T) curve from 300 to 800 K of the BTFO ceramic sample was measured at an applied field of 1 T. The M-T curve, which is the characteristic of ferromagnetism, shows a magnetic transition temperature (T_{FM}) around 680 K, which is higher than most of the current MF materials. The magnetization gradually drops as the temperature increases from 300 to 600 K. The inverse magnetization-temperature ($1/M$-T) curve is

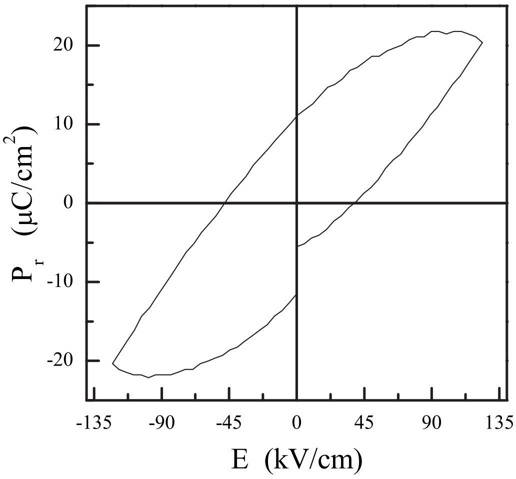

FIG. 4. The ferroelectric hysteresis loop of the $BaTi_{0.95}Fe_{0.05}O_{3-\delta}$ ceramics.

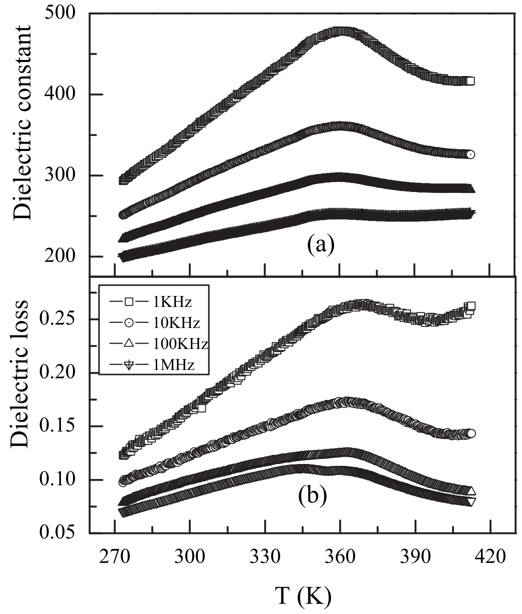

FIG. 5. The temperature dependence of dielectric constant and dielectric loss of the $BaTi_{0.95}Fe_{0.05}O_{3-\delta}$ ceramics at different frequencies, ranging from 100 Hz to 1 MHz.

also shown in the inset of Fig. 6. The high-temperature data, from 690 to 740 K, were fitted to the Curie-Weiss law from which θ_p was determined as 670 K. The θ_p obtained from the present Curie-Weiss fit should only be taken as an approximation because the small temperature range used is very close to the magnetic-ordering temperature.

At the ferroelectric transition temperature (365 K), the *M-T* curve shows no changes as shown in Fig. 6. The coupling between the ferromagnetism and ferroelectricity should be weak; otherwise there would be some change around the ferroelectric transition temperature.

The field dependence of the magnetization of the BTFO ceramics with a maximum magnetic field of 1.7 T is also shown in the inset of Fig. 6. The plot of *M* versus *H* shows a rather large magnetic hysteresis loop at the room temperature, indicating a ferromagnetic behavior. Above the magnetic transition temperature of 680 K, however, the *M-H* curve shows linear paramagnetic behavior. In this research, the highest saturated magnetization (M_s) is calculated to be as large as $0.75\mu_B/\mathrm{Fe}$ atom, assuming that all the Fe atoms contribute to the magnetization. This experimental value is much smaller than our calculated magnetic moment. The conflict between the magnetic moments obtained from the experiment and the calculation may be explained as follows. One of the possible reasons is that the calculations are carried out at $T=0$ K with Fe^{3+} ions distributed orderly, and that the Fe^{3+} ions distributed disorderly should be another possible reason.

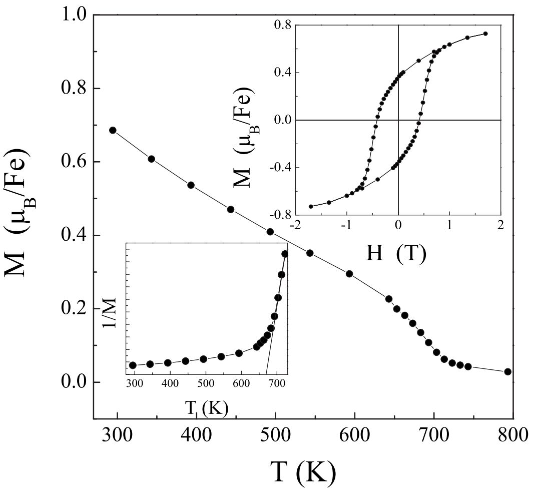

FIG. 6. The temperature dependence of the magnetization for $BaTi_{0.95}Fe_{0.05}O_{3-\delta}$ ceramics; the insets show a plot of $1/M$ versus temperature and the magnetic hysteresis loop of the $BaTi_{0.95}Fe_{0.05}O_{3-\delta}$ ceramics at room temperature.

Gemming and Schreiber[27] showed the effect of the geometry with the Fe at the $SrTiO_3$ boundaries. But the formation of significant amounts of iron oxides is ruled out by considering the structure determined by the XRD, HRTEM, and the magnetic properties in our results. Iron oxide peaks are not observed in the BTFO ceramics from XRD, and there are no detectable traces of any secondary phase or cluster of any oxide of iron by the HRTEM image and the EDX analysis taken from several arbitrary regions of the ceramic sample. The possible magnetic impurity phases in the system are γ-Fe_2O_3 and Fe_3O_4. The well-defined T_{FM} can be observed from the *M-T* curve as shown in Fig. 6 with $T_{FM}=680$ K for BTFO. The T_{FM} of BTFO is clearly different from those of two most likely impurity phases, γ-Fe_2O_3 (900 K) and Fe_3O_4 (850 K). The coercive field (H_C=4100 Oe) of the sample measured at the room temperature is much larger than those of γ-Fe_2O_3 (about 450 Oe) and Fe_3O_4 (about 25 Oe). If impurity phases of γ-Fe_2O_3 and Fe_3O_4 are responsible for the observed magnetism in the sample, one would have to assume that almost 50% of the doped Fe ions should be employed to form γ-Fe_2O_3 or Fe_3O_4 since the saturated magnetic moment of γ-Fe_2O_3 and Fe_3O_4 are reported to be $1.25\mu_B/\mathrm{Fe}$ and $1.3\mu_B/\mathrm{Fe}$,[28] respectively. If such a large amount of iron oxides were present, the significant XRD peaks or the secondary phase or cluster in HRTEM image of the γ-Fe_2O_3 or F_3O_4 would appear. These facts together systematically rule out the possibility that the observed ferromagnetism in the Fe-doped $BaTiO_3$ comes from the ferromagnetic γ-Fe_2O_3 and Fe_3O_4.

It is reasonable that the $BaTiO_3$ doped with Fe ions should be *n*-type semiconductor with the oxygen vacancy in the ceramics. The *n*-type carriers in the ceramic sample suggest that the mechanism responsible for the ferromagnetism should be related to electron-mediated Zener-type Ruderman-Kittel-Kasuya-Yosida interaction.[29] The substitution of Fe atom at Ti site in $BaTiO_3$ introduces the hybridization between the *p* orbital of O atom and the *d* orbital of the Fe atom in BTFO ceramics, similar to the *p-d* hybridization in DMS. This *p-d* interaction leads to the appearance of the additional mixed band levels derived from the $BaTiO_3$ valence band. According to such a model, electrons are in favor of mediating the exchange interaction between local moments and inducing the ferromagnetism, and the carriers in the BTFO ceramic result in the leakage current.

In summary, we designed a ferromagnetic and ferroelectric material Fe-doped $BaTiO_3$, and investigated its magnetic and dielectric properties. The ferromagnetic and ferroelectric transition temperatures are identified at about 670 and 365 K, respectively. We get reasonable large saturated magnetization and considerable remnant polarization. The appearance of both the ferromagnetism and the ferroelectricity in the Fe-doped $BaTiO_3$ ceramics at the room temperature implies that the Fe-doped $BaTiO_3$ may have potential application as MF materials in the future, and doping transition-metal ions into the wide-band-gap perovskite ferroelectrics, such as $PbTiO_3$ and PZT ($PbZr_xTi_{1-x}O_3$), may be a new way to develop the MF materials.

This work was supported by the Natural Science Foundation of China (Contract No. 50572036), the 973 projects (Contracts No. 2006CB921803 and No. 2009CB929503), and the grant of Education Ministry of China (Grant No. 20070284019). X.G.W. also wants to thank the Fok Ying Tung Education Foundation for the financial support through Contract No. 114010.

---

*jyin@nju.edu.cn

[1] J. F. Scott, Nature Mater. **6**, 256 (2007).

[2] M. Gajek, M. Bibes, S. Fusil, K. Bouzehouane, J. Fontcuberta, A. Barthelemy, and A. Fert, Nature Mater. **6**, 296 (2007).

[3] E. Ascher, H. Rieder, H. Schmid, and H. Stössel, J. Appl. Phys. **37**, 1404 (1966).

[4] J. Wang, J. B. Neaton, H. Zheng, V. Nagarajan, S. B. Ogale, B. Liu, D. Viehland, V. Vaithyanathan, D. G. Schlom, U. V. Waghmare, N. A. Spaldin, K. M. Rabe, M. Wuttig, and R. Ramesh, Science **299**, 1719 (2003).

[5] J. Hemberger, P. Lunkenheimer, R. Fichtl, H. A. K. Von Nidda, V. Tsurkan, and A. Loidl, Nature (London) **434**, 364 (2005).

[6] N. Ikeda, H. Ohsumi, K. Ohwada, K. Ishii, T. Inami, K. Kakurai, Y. Murakami, Y. Yoshii, S. Mori, Y. Horribe, and H. Kito, Nature (London) **436**, 1136 (2005).

[7] K. Saito and K. Kohn, J. Phys.: Condens. Matter **7**, 2855 (1995).

[8] N. Hur, S. Park, P. A. Sharma, S. Guha, and S. W. Cheong, Phys. Rev. Lett. **93**, 107207 (2004).

[9] T. Kimura, S. Kawamoto, I. Yamada, M. Azuma, M. Takano, and Y. Tokura, Phys. Rev. B **67**, 180401(R) (2003).

[10] Z. J. Huang, Y. Cao, Y. Y. Sun, Y. Y. Xue, and C. W. Chu, Phys. Rev. B **56**, 2623 (1997).

[11] N. Hur, S. Park, P. A. Sharma, J. S. Ahn, S. Guha, and S. W. Cheong, Nature (London) **429**, 392 (2004).

[12] S. W. Cheong and M. Mostovoy, Nature Mater. **6**, 13 (2007).

[13] R. Ramesh and N. A. Spaldin, Nature Mater. **6**, 21 (2007).

[14] W. Prellier, M. P. Singh, and P. Murugavel, J. Phys.: Condens. Matter **17**, R803 (2005).

[15] K. Ueda, H. Tabata, and T. Kawai, Appl. Phys. Lett. **79**, 988 (2001).

[16] S. B. Ogale, R. J. Choudhary, J. P. Buban, S. E. Lofland, S. R. Shinde, S. N. Kale, V. N. Kulkarni, J. Higgins, C. Lanci, J. R. Simpson, N. D. Browning, S. Das Sarma, H. D. Drew, R. L. Greene, and T. Venkatesan, Phys. Rev. Lett. **91**, 077205 (2003).

[17] J. Y. Kim, J. H. Park, B. G. Park, H. J. Noh, S. J. Oh, J. S. Yang, D. H. Kim, S. D. Bu, T. W. Noh, H. J. Lin, H. H. Hsieh, and C. T. Chen, Phys. Rev. Lett. **90**, 017401 (2003).

[18] T. Dietl, H. Ohno, F. Matsukura, J. Cibert, and D. Ferrand, Science **287**, 1019 (2000).

[19] Z. Chao, C. L. Wang, J. C. Li, and K. Yang, Chin. Phys. **16**, 1422 (2007).

[20] P. E. Blochl, Phys. Rev. B **50**, 17953 (1994).

[21] G. Kresse and J. Hafner, Phys. Rev. B **47**, 558 (1993).

[22] G. Kresse and J. Furthmüller, Comput. Mater. Sci. **6**, 15 (1996).

[23] G. Kresse and J. Furthmüller, Phys. Rev. B **54**, 11169 (1996).

[24] V. Anisimov, F. Aryasetiawan, and A. Lichtenstein, J. Phys.: Condens. Matter **9**, 767 (1997).

[25] A. Jana, T. K. Kundu, S. K. Pradhan, and D. Chakavorty, J. Appl. Phys. **97**, 044311 (2005).

[26] W. Martienssen and H. Warlimont, *Springer Handbook of Condensed Matter and Materials Data* (Springer, Berlin, 2005).

[27] S. Gemming and M. Schreiber, Chem. Phys. **309**, 3 (2005).

[28] R. C. O'Handley, *Modern Magnetic Materials: Principles and Applications* (Wiley, New York, 2000).

[29] T. Dietl, H. Ohno, F. Matsukura, J. Cibert, and D. Ferrand, Science **287**, 1019 (2000).